# 1.2. NUCLEAR PHYSICS WITH NEUTRONS

## 1. Introduction

In the reported period, the experimental research program of FLNP included traditional directions: experimental investigations of the fundamental properties of the neutron, studies of the processes of spatial parity violation in different nuclear reactions induced by neutrons, investigations of highly excited states of nuclei in reactions with resonance and fast neutrons, astrophysical aspects of neutron physics, experiments with ultracold neutrons. An extensive program of studies in resonance neutron induced fission was partly completed.

Also, experimental approaches in such a fundamental field as time-noninvariance effects in the interaction of resonance neutrons with nuclei are under investigation. At present, the study of polarized neutron propagation through polarized targets seems to be the most convenient way of direct tests of time-reversal invariance.

Applied research in the field of neutron activation analysis (NAA) and also, a methodological development of neutron and gamma detectors of different types were conducted.

The main part of these investigations was carried out on seven neutron beams of the IBR-30 booster, the first and eleventh beam of the IBR-2 reactor, and the experimental facility "Regata" for neutron activation analysis at IBR-2. At the same time, a number of works were conducted in collaboration with the nuclear centers of Russia (RRC KI, ITEP, MEPI, PNPI, PEI, RSRIEP), Ukraine (INR NU, Kiev), Bulgaria (INRNE, Sofia), Poland (UL, Lodz; INP, Krakow), Germany (FZK, Karlsruhe; Tubingen Univ.; THD, Darmstadt; FRM, Garching), Republic of Korea (PAL, Pohang; KAERI, Taejon), France (ILL, Grenoble; CEC CEA, Cadarache), Belgium (IRMM, Geel), USA (LANL, Los Alamos), China (Peking University) and Japan (Kyoto University; KEK, Tsukuba) at their neutron sources. It is necessary to note that the new opportunities which opened after Russia had jointed ILL, Grenoble have been effectively used: some measurements with cold and ultracold neutrons were successfully performed.

Very interesting possibilities for investigations are opening now in the framework of a wide international collaboration PS-213 based on a new n-TOF facility which starts operation in late May 2000 in CERN.

The research program for IBR-30 was written taking into account the working schedule of the creation of the new Intense REsonance Neutron source for nuclear physics investigations — the IREN project. In accordance with the recently revised schedule approved in March 1999 by the JINR directorate, the IREN source is to start operation by the end of 2002. So, the complex IBR-30+LUE-40 has to be dismounted in the second half of 2001. A very important reason why the IBR-30 scientific program has continued to present and will continue in nearest future is to preserve the research team able to carry out investigations on the basis of the IREN source and prepare new experimental techniques for such investigations.

## 2. Experimental Researches

### *2.1. Parity Violation in the Interaction of Resonance Neutrons with Nuclei*

#### 2.1.1. TRIPLE collaboration results

The Frank Laboratory of Neutron Physics participates in the Time Reversal Invariance and Parity at Low Energy (TRIPLE) collaboration studying Parity NonConservation (PNC) in compound-nuclear states. The experiments are conducted at the Los Alamos pulsed neutron source LANSCE by the transmission of longitudinally polarized neutrons through isotopically pure targets. The directly measured quantities are the longitudinal asymmetries of the cross sections for p-wave resonances defined as $\sigma_p^{\pm} = \sigma_p(1 \pm p)$, where $\sigma_p^{\pm}$ is the resonance cross section for positive and

negative neutron helicities, $\sigma_p$ is the resonance part of the p-wave cross section. In the statistical approach, a set of PNC matrix elements obtained for many resonances determines the mean square matrix element $M^2$ of the effective weak interaction of nucleons in nuclei provided that complete spectroscopic information about resonances is obtained in addition to longitudinal asymmetries. Dividing the level spacing by $D$ one obtains the weak spreading width $\Gamma_w = 2\pi M^2/D$ which is a global measure of the strength of the effective parity violation interaction in nuclei; it has a typical value of ~$10^{-7}$ eV. In 1999 the $\Gamma_w$ results were published for $^{93}$Nb, $^{103}$Rh, $^{107,109}$Ag $^{106;108}$Pd and $^{133}$Cs. They are shown in Table 1.

*Table 1*

| Nuclei | $^{93}$Nb | $^{103}$Rh | $^{106}$Pd | $^{107}$Ag | $^{108}$Pd | $^{109}$Ag | $^{133}$Cs |
|---|---|---|---|---|---|---|---|
| $\Gamma_w(10^{-7}$ eV) | **≤ 0.11** | $1.4^{+1.2}_{-0.6}$ | $34.0^{+47.0}_{-28.0}$ | $2.7^{+2.6}_{-1.2}$ | **≤ 12.0** | $1.3^{+2.5}_{-0.7}$ | $0.006^{+0.154}_{-0.003}$ |

The data indicate possible existence of local fluctuations in the mass dependence of the weak interaction in compound nuclei contrary to an earlier conclusion about the mass independence of the weak interaction spreading width [FLNP Annual Report 1998, p.17].

## 2.2. *Experimental Approaches to Time-Noninvariance Effects in the Interaction of Resonance Neutrons with Nuclei*

### 2.2.1. Comparative analysis of experimental proposals on T-, P-invariance tests in nuclear reactions with neutrons.

An analysis of different proposed experiments to investigate CP-violation in nuclear reactions induced by resonance neutrons was carried out. The formalism of spin density matrices and special methods of the nuclear reaction theory were used to analyze the CP-violating quantities suggested for measurement in various experiments. The dependence of the effects and their relative errors on the neutron energy and target thickness was studied. The necessity to compensate strong pseudo-magnetic precession by an external magnetic field is shown. Being completely compensated some of the above effects show an additional enhancement of 3 orders of magnitude while the total enhancement reaches 6 orders of magnitude. In this case, neutron spin reverse essential for the effect occurs due to precession caused by the CP-violating interaction while the beam absorption is caused by the strong nuclear interaction. The enhancement appears due to the dynamical and resonance mechanisms caused by a complicated (chaotic) structure of compound resonances. An analysis of some other relevant quantities shows that, although their values themselves do not show resonance enhancement, their relative errors decrease sharply in the vicinity of the p-wave resonance.

To avoid some problems mentioned above, one can use a two-stage scheme with just one neutron polarization device proposed in FLNP.

Nowadays, there are two possible target designs for the proposed experiment. The first is the Dynamical Nuclear Polarization technique for the polarization of $^{139}$La nuclei in a $LaAlO_3$ compound. It requires extra-low temperatures and a high magnetic field. The second is the optical polarization of $^{131}$Xe in exactly the same manner as $^3$He. The latter is precisely the experimental approach that is now under investigation within the KaTRIn project.

### 2.2.2. Recent results of the KaTRIn project

The ability to create a long-lived high nuclear spin polarization in dense noble gases ($^3$He, $^{129}$Xe, $^{131}$Xe) opens wide perspectives in new fundamental and applied research and medicine applications. We propose to use a spin-polarized $^3$He nuclear target as a neutron

polarizer and analyzer of neutron polarization in the KaTRIn project for an experimental test of time-reversal invariance in nuclear reactions. A high polarization in the neutron beam can be reached by the use of the dense ($3 \cdot 10^{20}$) highly polarized (~50%) prolonged Ø3x30 $cm^3$ $^3He$ target. The spin exchange technique allows the creation of high nuclear polarization directly in dense noble gases by transferring the electron spin of optically pumped alkali (Rb, K, Cs) atoms. As nuclear polarization cannot be higher than electron polarization and the growing rate of nuclear polarization is proportional to the alkali atom number density, a powerful circularly polarized laser beam tuned to the atomic resonance line is required. In 1999, an experimental setup for creating a $^3He$ neutron target (Figure 1) was built. To have high polarization values, $P_{Rb}$, the laser should provide no less than 0.2 W per every $cm^3$ of Rb vapor at density $n_{Rb} \approx 10^{15}$ $cm^{-3}$. In recent years, powerful diode laser arrays with the power up to 30 W became available. We used 15 W 23, a diode laser array, tuned to the D1 Rb resonance line (795 nm). The laser spectrum was thoroughly investigated using a spectrograph.

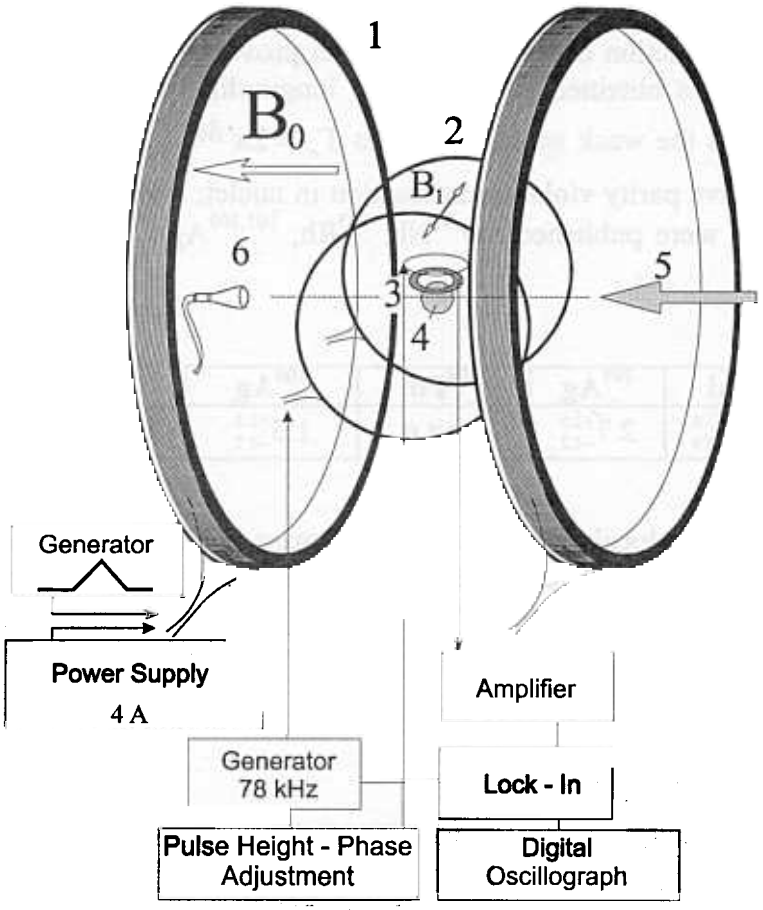


*Fig. 1. NMR system: 1- Helmholz coils, 2- RF-coils, 3- Pick-up, 4- $^3He$ Cell, 5- Laser beam, 6- Photodiode*

We investigated three spherical cells with the diameters 2 cm (A), 4 cm (B), and 3 cm (C) filled with at 2, 8.5, and 13 atm, respectively. The cells were heated up to 200 C° and the averaged polarization was determined from the absorption spectra using the spectroscopic technique by switching the stabilizing magnetic field on and off. The experimental data are supported by the calculations based on the numerical solution of the equations describing broadband light propagation through an optically dense medium.

The $^3He$ nuclear polarization, $P_{He}$, was determined by a standard technique of NMR adiabatic fast passage. Helmolz Ø1400 mm coils produced an axial stabilizing magnetic field of 22.4 Gauss along the laser beam direction with a homogeneity not worse than in the middle and variations in time being at the same level. A pair of radio frequency (RF) coils 700 mm in diameter produced a 78 kHz transverse field.

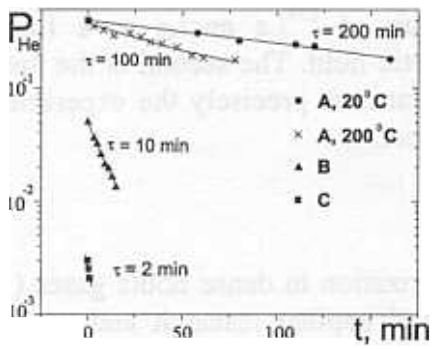


*Fig. 2. $^3He$ nuclear polarization decay curves*

A saw-like pulse of 3 Gauss was applied to the stabilizing field to create resonance conditions for $^3He$ nuclei. NMR pick-up coils were incorporated into a cell holding platform. Their axis was orthogonal to the stabilizing and RF-field. The induced NMR signal was guided to lock-in the amplifier and then to the digital oscilloscope. The sensitivity of the system was about

$5 \cdot 10^4$ V/Gauss. The RF - interference and vibrations, set the noise level at about 100 mV. The value of $P_{He}$ was indirectly determined by the calculation of the filling factor and is shown in Figure 2. Rather low decay constants, $\tau$, can be attributed to cell wall relaxation and paramagnetic impurities in $^3$He. Nevertheless, the efficiency of polarization transfer happened to be rather high, about $10^{18}$ of $^3$He atoms/s for a B cell. Generally, Helmholz coils and the related equipment are necessary for the NMR measurement of the $^3$He polarization. On the other side, it can be extracted from measurements in the neutron beam. The μ-metal magnetic shields can provide a homogeneous magnetic environment for the $^3$He target. Now, this activity is underway and the first experimental tests on an IBR-30 neutron beam will be conducted in 2000.

### 2.3. *Theoretical and experimental approaches to studies of the amplitude of the n-e interaction and the electric polarizability of the neutron*

Methodological experiments and MC calculations have been carried out at IBR-2 to optimize the scheme of the experiment to study the neutron elastic cross section on noble gases with the aim of extracting the neutron-electron scattering length. It was observed that the neutron beam from the IBR-2 reactor passing through a mirror neutron guide becomes inhomogeneous in energy. This fact causes serious experimental difficulties in the measuring of the angular anisotropy of the scattered neutrons on a Xe target. However, computations show the possibility of the extraction of the (n, e) scattering length from measurements of the elastically scattered neutron intensity in the $4\pi$-geometry if one uses a gaseous Ar target. The advantage of Ar is its relatively small nuclear scattering cross section resulting in a relative contribution of the (n, e) scattering equal to Xe's.

In the year 2000 a high-pressure Ar-filled gaseous chamber with $^3$He proportional counters around it will be constructed and the first measurements of the Ar scattering cross section will be carried out.

A new method to study the neutron polarizability and neutron–electron scattering was proposed. It is based on the fact that the real part of the s-wave scattering amplitude changes its sign near the s-wave neutron resonance at $E = E^* = E_0 - \frac{\Gamma_n}{2kR_0'}$ (here $E$ is the neutron energy, $E_0$ is the energy of the resonance, $k$ and $\Gamma_n$ are the resonant values of the neutron wave number and width, $R_0'$ is the s-wave scattering radius). The method consists of the observation of the energy behavior of the forward–backward scattering asymmetry $\omega_1 = \frac{\sigma(\vartheta_1) - \sigma(\vartheta_2)}{\sigma(\vartheta_1) + \sigma(\vartheta_2)}$ that experiences a jump at $E=E^*$, here $\sigma(\vartheta)$ is the differential scattering cross section. Approximate expressions for the differential cross section are presented by the equation $\sigma(\vartheta) = (f_0 + f_1 \cos\vartheta + a_{ne} Zf(q))^2$, where $f_0$ is the s- wave scattering amplitude, $f_1 = f_1^N + f_1^{pol}$ is the sum of nuclear and polarizability contributions to the p-wave amplitude, $a_{ne} = (1.3-1.6) \cdot 10^{-3} fm$, $f(q)$ is the atomic formfactor, $q = 2k\sin\frac{\vartheta}{2}$ is the transferred momentum. Thus, in the expression for $\sigma(\vartheta)$ we have the interference terms $2f_0 f_1 \cos\vartheta$ and $2f_0 a_{ne} Zf(q)$. The calculations show that the latter term for $Z \geq 70$ and $1\text{eV} \leq E \leq 10eV$ exceeds $2f_0 f_1$ ~100 times. It makes $\omega_1$ be always negative at energies below $E^*$ and positive at energies higher than $E^*$. It is supposed that this phenomenon will serve as a new method for the observation of $a_{ne}$. More detailed calculations of possible experiments to investigate $a_{ne}$ will be done.

## 2.4. *Interference Effects in Resonance Neutron Induced Nuclear Fission and Delayed Neutron Yields at Thermal Energy*

### 2.4.1. Angular correlations of fission fragments in the resonance neutron induced fission of the $^{235}$U nucleus

Spontaneous and induced nuclear fission has been under investigation for over 50 years but we do not have a complete understanding of its mechanism and dynamics yet. This is because nuclear fission is one of the most complicated nuclear transformations connected with deep rearrangement of the mass and charge of initial nuclei, production of extremely deformed and excited fragments with high spin and excitation energy sufficient for the emission of several neutrons and about ten gamma quanta. Another basic circumstance is the fact that in most cases, nuclear fission is studied in the conditions when it is impossible to obtain information on basic amplitudes of the process. Such amplitudes are characterized by the parity $\pi$ of the system, its spin $J$ and the projection on the fission axis $K$. Resonance $s$- or $p$-neutron induced fission only permits one to obtain information on $J^{\pi}K$ fission amplitudes because in the total cross section of the (n, f) reaction and in the energy dependence of the angular distribution of fission fragments there appears the interference of $J^{\pi}K$ amplitudes of different compound states. The possibility of the extraction of fission amplitudes from the experiment with an aligned $^{235}$U target is determined by the existence of a complete set of experimental data on differential and total cross sections for this nucleus.

In 1999, data taking in the experiment to measure the fission fragment angular anisotropy of the $^{235}$U resonance neutron induced fission with an aligned $^{235}$U target in the energy region 0.5–30 eV finished. The value of the anisotropy coefficient $A_2$ $(E)$ was extracted. The energy dependence of the $A_2$ coefficient, which characterizes the angular anisotropy of fission fragments, is shown in Fig.3.

For a combined analysis, the experimental cross sections for $^{235}$U available from the National Nuclear Data Center (NNDC) at BNL were used. All other cross sections are also well reproduced. The dashed line is calculated using a set of resonance parameters from the ENDF/B-VI library, which also describes all other cross sections quite well, but obviously

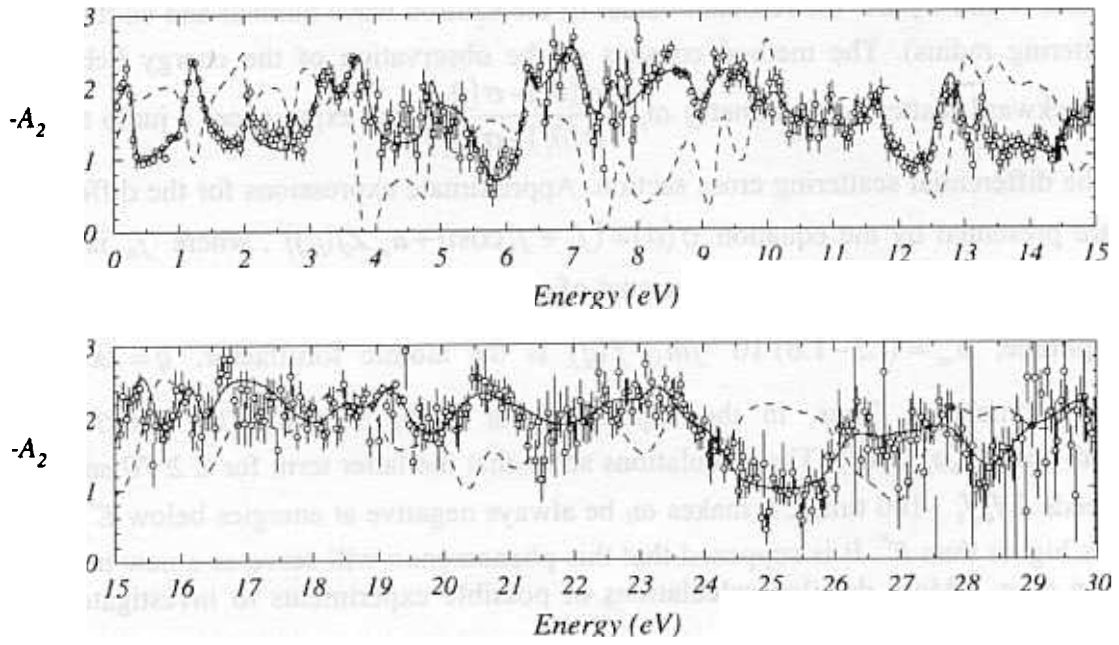


*Fig. 3. The results of the fit (solid curve) for $A_2$ (E), circles are the experimental data. The dashed line is calculated using the resonance parameters from ENDF/B-VI.*

fails to reproduce the $A_2$ energy dependence. It is necessary to note that the latter set of resonance parameters was obtained in the two-channel approximation without taking into account the information on $A_2$ (E).

The data were analyzed assuming that three channels are open for the spin group $J=3$ ($K=0,1,2$) and two for the spin group $J=4$ ($K=1,2$). According to a commonly used assumption the $J^{\pi}K=4^{-}0$ state is forbidden by parity conservation. We can expect no or a very small contribution from higher $K$ states ($J^{\pi}K=3^{-}3$, $4^{-}3$, and $4^{-}4$) as the geometrical factors defining the value of the anisotropy coefficient for these fission channels have a positive sign while the observed anisotropy coefficient $A_2$ is negative over the whole measured energy range. The fission barriers for these states should be much higher. So these fission channels are not taken into account. The integral distributions of the partial fission widths for the spin group $J=4$ obtained in such approximation turned out to be not consistent with the Porter-Thomas distribution with one degree of freedom (see Fig. 4, right column). An additional fission channel seems to be open for this spin group. It is necessary to note that the conclusion about an absolute forbiddeness of the $4^{-}0$ channel was based on A.Bohr's hypothesis in its simplest variant. However, a more careful examination of the problem leads to a conclusion that the $4^{-}0$ channel has a higher first fission barrier and a relatively low second one for asymmetric fission modes. Thus, one would expect the $J^{\pi}K=4^{-}0$ channel to be at least partially open in our case. So, we reanalyzed the data assuming that all three channels are open for both spin groups.

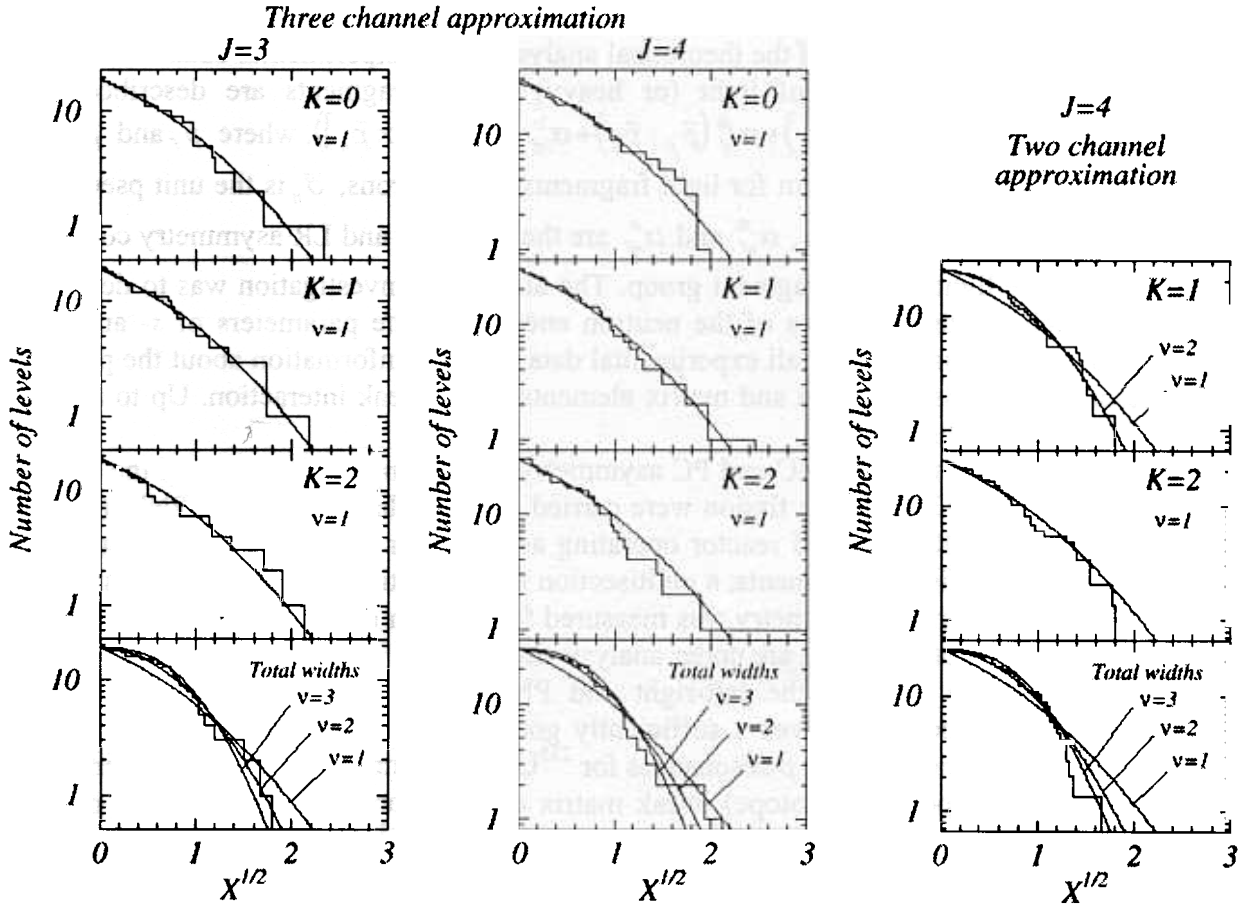


*Fig. 4. Integral distributions of partial and total fission widths (number of resonances with* $\Gamma_{\lambda f}/\langle\Gamma_{\lambda f}\rangle > X$*). Solid lines are the* $\chi^2$ *distributions with* $\nu$ *degrees of freedom.*

For more details see the section of scientific publications: "Angular Anisotropy of Fission Fragments from the Resonance Neutron Induced Fission of an Aligned $^{235}$U Target and the Role of $J^{\pi}K$ Fission Channels".

In 2000, experiments to study the angular anisotropy of fission fragments for different mass groups will continue. Also, experiments to determine the temperature dependence of the anisotropy coefficient will be done aiming at an increase of the accuracy of the absolute value of the anisotropy coefficient.

### 2.4.2. Parity violation and other effects caused by the interference of *s*- and *p*- wave neutron induced fission

To explain PNC effects in nuclear fission, theoreticians used an assumption about neighboring compound-states with opposite parities mixed by the weak nucleon-nucleon interaction. As it is well known, an analogous assumption was used earlier to explain the PNC-effect arising in the (n, γ) - reactions.

As a result of such a mixing, the interference between the fission channels with equal values of ***JK*** and opposite parities may arise. In turn, this interference leads to the asymmetry of light (heavy) fragment emission relative to the spin direction of the polarized neutrons initiating the nuclear fission.

Recently on the basis of a consistent theory of neutron-induced fission it was shown that parity conserving (PC interference effects such as the left-right (LR) and forward-backward (FB) asymmetry of fission products emission could be expressed through the same fission amplitudes as the PNC effect. As a result, complementary investigations of PNC and PC interference effects can essentially extend the capabilities of the theoretical analysis of the experimental data.

The angular distributions of light (or heavy) fission fragments are described by the expression: $W(\vec{p}_f)=1+\alpha_{nf}(\vec{\sigma}_n\cdot\vec{p}_f)+\alpha_{nf}^{fb}(\vec{p}_f\cdot\vec{p}_n)+\alpha_{nf}^{lr}\cdot(\vec{p}_f\cdot[\vec{\sigma}_n\times\vec{p}_n])$, where $\vec{p}_f$ and $\vec{p}_n$ are the unit vectors of the linear momentum for light fragments and neutrons, $\vec{\sigma}_n$ is the unit pseudovector of the neutron polarization, and $\alpha_{nf}$, $\alpha_{nf}^{fb}$ and $\alpha_{nf}^{lr}$ are the PNC, FB and LR asymmetry coefficients, respectively, for the light fission fragment group. The aim of the investigation was to determine $\alpha$ coefficients which are the functions of the neutron energy and the parameters of *s*- and *p*-wave resonances. Simultaneous fitting of all experimental data can give information about the parameters of the *p*-resonances of fissile nuclei and matrix elements of the weak interaction. Up to now, such information is entirely absent.

All measurements of the PNC and PC asymmetry coefficients as functions of the resonance neutron energy in $^{233,235}$U and $^{239}$Pu fission were carried out in collaboration with PNPI (Gatchina) on the beams of the IBR-30 pulsed reactor operating as a booster with a LUE-40 electron linear accelerator. To register fission fragments, a multisection fast ionization chamber was constructed.

In 1999, the left-right asymmetry was measured for $^{239}$Pu in the energy region from thermal neutron to 70 eV. The obtained data are under analysis now.

For $^{233,235}$U, the data on the left-right and PNC effects were analyzed. Simultaneous processing of the obtained data gives a sufficiently good description of the observed effects. In doing so, tentative parameters of 29 *p*-resonances for $^{235}$U and 18 ones for $^{233}$U were obtained. For 6 uranium resonances (3 per each isotope), weak matrix elements are estimated and the mixing of states with different parities is obtained. The value appears to be $10^{-4} - 10^{-3}$ eV.

### 2.4.3. Delayed neutron yields

It is well known that the existence of delayed neutrons (DN) has a fundamental significance for the realization of a controllable chain fission reaction. The yields and time characteristics of DN from the main reactor isotopes, $^{235}$U, $^{239}$Pu and $^{233}$U, are some of the most important nuclear reactor constants used in kinetic calculations. An accuracy of 3% for $^{235}$U, 4% for $^{239}$Pu and 6% for $^{233}$U

has now been achieved for DN yields. Nevertheless, the requirements for the accuracy of the parameters have continued to increase.

The measurements of the $\beta_0 = \frac{\nu_d}{\nu_d + \nu_p}$ values for the thermal neutron induced fission of $^{233}U$, $^{235}U$, $^{239}Pu$ and $^{237}Np$ isotopes were performed with an ISOMER facility at IBR-2. Here, $\nu_d$ is the number of DN, and $\nu_p$ is the number of prompt neutrons. The IBR-2 operation mode, the pulse rate 5 Hz, permits one to register neutrons in a 200 ms time period. The system of a chopper synchronized with the reactor pulses allows one to extend the time interval to 800 ms by rejecting one or two reactor pulses and irradiating the sample with neutrons from a selected energy region.

The DN yields from $^{233}U$, $^{235}U$, and $^{239}Pu$ were measured after samples irradiation with neutrons of the energy 3 meV, 23 meV, or 40 meV. In the experiment the yields were measured relative to the DN yields at thermal neutron irradiation. The results on $\beta_0$ for 3 meV and 23 meV energies are presented in Table 2.

*Table 2*

**$\beta_0$ values (in %) and ratios to standard DN yields (from $^{235}U$ thermal neutron induced fission)**

| Isotope | En = 0.003 eV | En =0.023 eV |
|---|---|---|
| $^{235}U$ | 0.683 ± 0.021 (1.004 ±0.009) | 0.680 ± 0.021 (1.000) |
| $^{233}U$ | 0.274 ± 0.009 (0.403 ± 0.006) | 0.267 ± 0.009 (0.393 ± 0.006) |
| $^{239}Pu$ | 0.227 ± 0.011 (0.334 ± 0.016) | 0.234 ± 0.008 (0.344 ± 0.004) |

There is no energy dependence of $\beta$-values in the energy range between cold and thermal neutrons.

One can see that the accuracy of relative measurements is on the level of 1%. The errors of absolute values are determined by uncertainty in the DN yield from $^{235}U$ which serves as a standard. The same experimental setup allows one to obtain the time dependence of the DN yield in short periods of time (up to 800 ms).

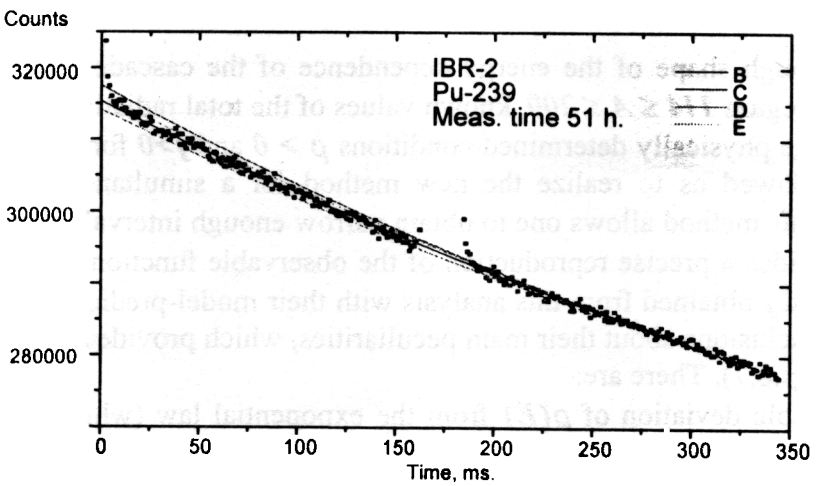


*Fig. 5. DNs from the $^{235}U$ experimental points and calculations in the 6-group approach.*

Figure 5 represents the experimental results for the $^{235}U$ DN yield time dependence. The statistical accuracy is 0.2 - 0.3% in a 1 ms time interval. The experimental data are compared with the calculation using the 6-group approach with group constants from different authors.

For $^{237}Np$, two different methods of $\beta_0$ determination were used. The results for $\nu_d$ are 1.25±0.11 and 1.14±0.09. One should mention that measurements of the $\nu_d$ value for $^{237}Np$ in the thermal energy region were performed for the first time thanks to using a unique combination of a large high purity Np sample and the neutron beam cleaned from fast neutrons.

#### 2.4.4. Studying of fission modes and their correlations with the quantum numbers of compound states

A method of precise measurements of the kinetic energies of fission fragments was developed and realized for actinide isotopes. The method is based on a double ionization chamber with Frish grids. Using the method TKE were measured for low lying $^{235}U$ resonances with a statistical accuracy of one order of magnitude better than in previous works. This enabled measurements of TKE in narrow energy bins of 0.2 eV in the energy region up to 10 eV. An analysis of the experimental results could give information on variations of fission mode weights as a function of excitation energy of the fissioning system.

### *2.5. Highly Excited States of Nuclei*

#### 2.5.1. Studying of the (n, 2γ) reaction

The acquisition, analysis and systematization of the experimental data on the properties of heavy enough (first of all, deformed) nuclei at the excitation energy $E_{ex} \leq B_n$ continued. Detailed and reliable information is necessary for a better understanding of the process of nuclear transition in this energy region from simple, well-studied structures to extremely complicated compound states. An analog of this process for a macroscopic system is a transition from order" to chaos". At present, maximum possible information on this process in any nucleus is only provided by the study of two-step γ-cascades proceeding between the compound state of the nucleus and its low-lying levels. The intensity of two-step cascades measured in the experiment equals the product of the radiative strength functions $f$ of the primary and secondary $E1$ and $M1$ transitions and the density $\rho$ of the states excited by them in the energy interval $\leq B_n$. A detailed study of nuclear parameters requires the measurement of these parameters with a high enough accuracy. This has stimulated the development of a new technique for the extraction of such data because all the algorithms of analysis used for this aim earlier have irremovable systematical uncertainties of an unknown magnitude.

A detailed enough shape of the energy dependence of the cascade intensity observed for nuclei from the mass region $114 \leq A \leq 200$, known values of the total radiative widths of compound states together with the physically determined conditions $\rho > 0$ and $f>0$ for any of excitation or γ-transition energies allowed us to realize the new method for a simultaneous estimation of the parameters $\rho$ and $f$. This method allows one to obtain narrow enough intervals of variations of the $\rho$ and $f$ values and provides a precise reproduction of the observable functionals of cascade γ-decay. A comparison of $\rho$ and $f$ obtained from this analysis with their model-predicted values allows us to make quite certain conclusions about their main peculiarities, which provides a precise reproduction of the experiment (Figs.6,7). There are:

1. A considerable deviation of $\rho(E)$ from the exponential law (which is characteristic for pure fermion systems) at the excitation energy of about 2 MeV. It is not excluded that $\rho(E)$ at this energy can have a constant value or even decrease with increasing excitation energy. The corresponding energy regions of this effect in nuclei of different types shift by approximately a value of the neutron pairing energy. The strongest demonstration of the effect of the "stepwise" structure is observed in deformed nuclei.

The conclusion about the existence of a serious deviation of $\rho$ from the exponential law in the excitation energy interval mentioned above is confirmed by an additional independent analysis. In this analysis, the distributions of random (due to their physical nature) deviations were approximated by some functions over a given excitation energy interval around the detection threshold $L_c$ of individual cascades with a further extrapolation of the result to the value $L_c = 0$. The density of the cascade intermediate levels unambiguously determines the shape of this distribution in the excitation energy interval under consideration. These results are shown in Fig.6, as well.

2. The sums of the strength functions $f(E1)+f(M1)$ which allow the description of all the measured functionals of the cascade γ-decay process deviate noticeably from the model predictions. The least discrepancy between theory and experiment is observed for low-energy transitions in near-magic nuclei provided a modified giant electric dipole resonance model in which the width of the resonance depends on the nuclear temperature and quantum energy is used. The majority of deformed nuclei demonstrate a considerable enhancement of the RSFs of high-energy transitions. An abrupt increase in the discrepancy is observed in the vicinity of double-magic nuclei (N = 126; Z = 82).

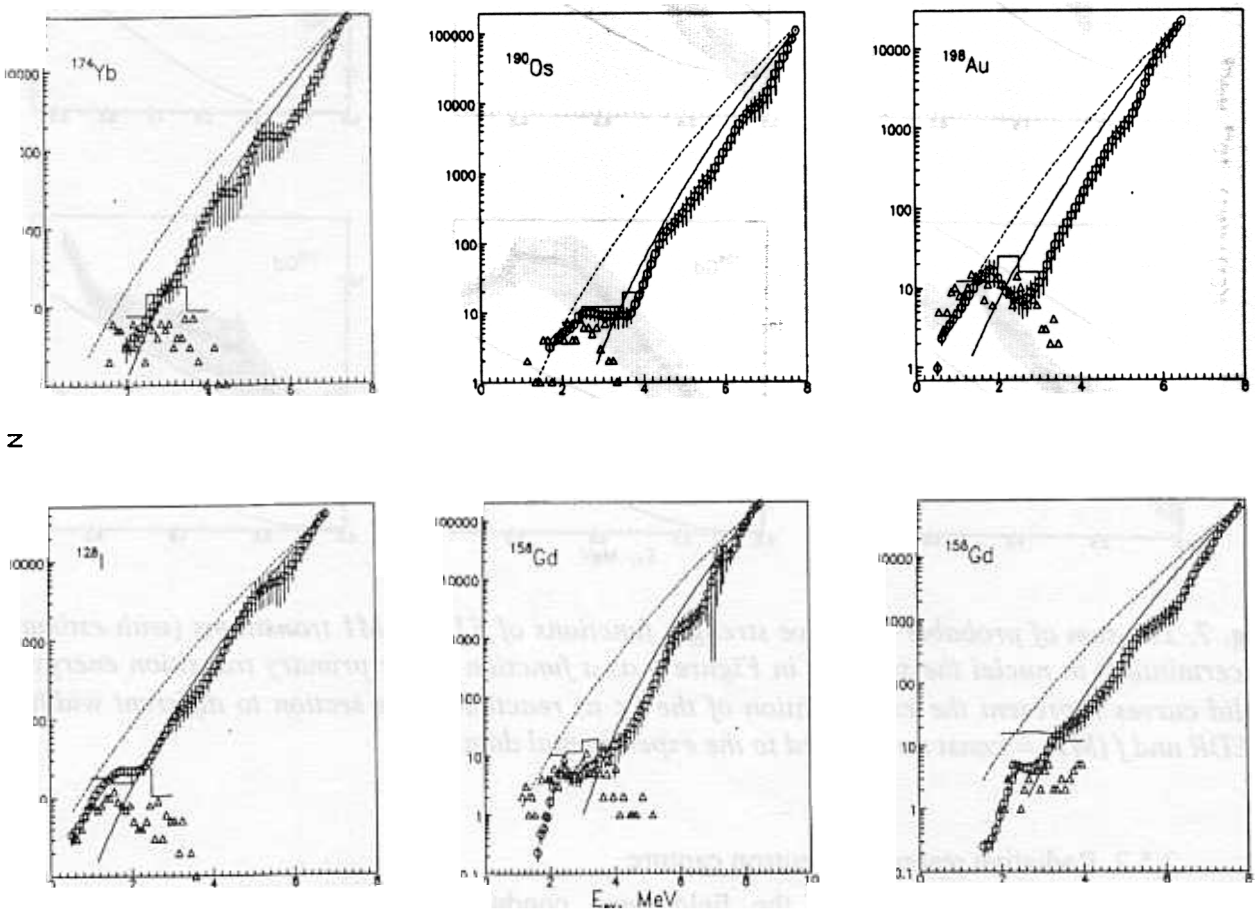


*Fig. 6. The number of levels of both parities excited by primary dipole transitions in 100 keV energy intervals as a function of the excitation energy $E_{ex}$. Triangles represent the experimental data, histogram is the estimation of the level density for a zero detection threshold, $L_c = 0$; points with bars are the most probable ρ values reproducing both cascade intensities and total radiative widths. Dashed and solid curves correspond to the Fermi-gas model and generalized model of a superfluid nucleus, respectively. The model parameters are chosen to reproduce the resonance spacing*

At present, the simplest qualitative explanation of the observed effects can be made under the assumption that the observed energy dependence of the level density above 3-4 MeV corresponds to the theoretical approach of the generalized model of the superfluid nucleus in its

early variant. This means that the structure of states in the excitation energy interval 1-2 to 3-4 MeV (and, probably, higher) must be mainly determined by vibrational (boson) components. The structures of levels at higher energies must be under dominant influence of quasiparticle (fermion) components.

This conclusion is confirmed by the observation of the regularity in the excitation spectra of the intermediate levels of the most intense cascades (equidistant period between 3, 4 and more levels equals some hundred keV).

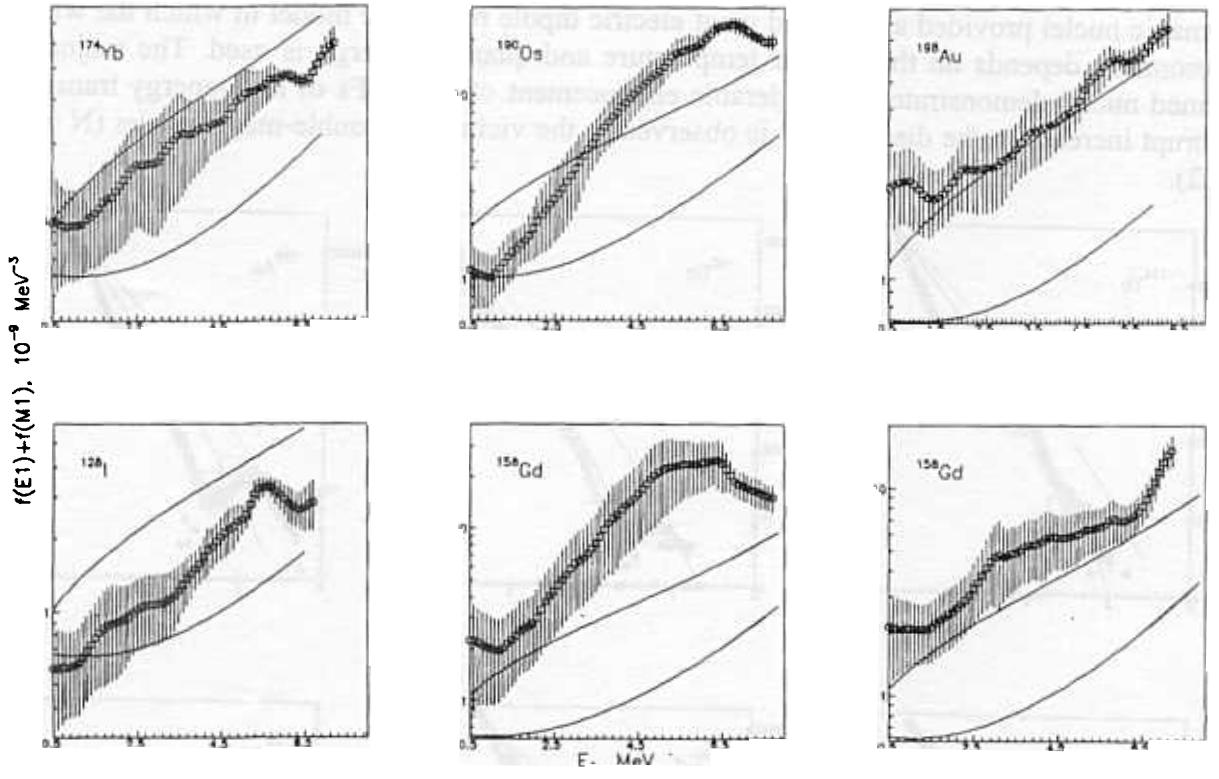


*Fig. 7. The sum of probable radiative strength functions of E1 and M1 transitions (with estimated uncertainties) in nuclei the same as in Figure 6 as a function of the primary transition energy $E_1$. Solid curves represent the extrapolation of the ($\gamma$, n) reaction cross section to different widths of GEDR and f (M1) = const normalized to the experimental data.*

2.5.2. Radiative resonance neutron capture

In 1999, investigations in the field were conducted in several directions using the ROMASHKA and PARUS multidetector facilities. On the ROMASHKA facility the measurements of gamma-quanta multiplicities and the determination of the parameters of neutron resonances: spins, radiative widths and neutron strength functions, and the mean gamma-ray multiplicity after resonance capture in $^{149}$Sm, $^{117}$Sn, $^{187}$Re, $^{232}$Th, $^{48}$Ti and after the fission of $^{235}$U and $^{239}$Pu isotopes over the energy interval from 20 to 300 eV were conducted. On the PARUS spectrometer similar measurements of the same isotopes plus $^{238}$U and Pb were done in the energy region from 4 to 160 eV.

Incomplete data on spins and radiative widths and a practical lack of information about gamma-spectra from the resonance neutron capture and fission of the mentioned nuclei determined the importance of the measurements. The radiative capture cross section of Hf, Sn, and In isotopes in the resonance neutron energy range is interesting from the point of view of the understanding of the process of nucleosynthesis. At the same time, these investigations have a certain applied

importance. Some of the above mentioned isotopes are used in reactor construction where new, more exact and reliable data are now necessary in connection with an increasing accuracy of nuclear reactor calculations. The data on the spectra of capture γ-rays are important for shielding calculations.

Pioneering experiments to measure the effects of resonance self-shielding and the value of $\alpha = \sigma_\gamma / \sigma_f$ for $^{235}U$ target nuclei in the 20-2000 eV energy region were performed. Multiplicity spectra were also measured for the $^{239}Pu$ target to refine the α- value for $^{239}Pu$ in the 0.007-20 keV energy region. As a result, α- values were obtained for 80 resonances and several energy groups.

In collaboration with Pohang Accelerator Laboratory (PAL, Pohang, Republic of Korea) group total cross sections were obtained. Transmission experiments were performed on the PARUS spectrometer with samples-filters of different thickness made from $^{232}Th$ and $^{237}Np$.

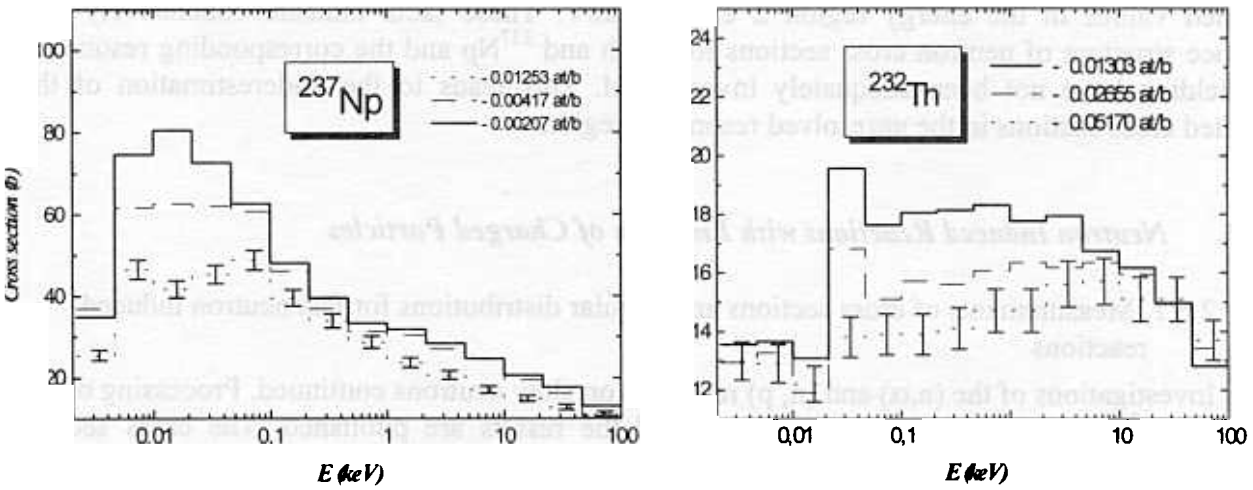


*Fig.8. The experimental total group cross-sections of $^{237}Np$ and $^{232}Th$ for different thickness of the sample.*

Figure 8 represents experimentally observed total group cross sections for $^{232}Th$ and $^{237}Np$. Figure 9 show a comparison between the experimental total cross section for the thickest samples and the calculated with the GRUKON code using the ENDF/B-6 and JENDL-3 libraries. The experimental uncertainties of the transmission coefficients range from 0.2% to 0.5% and the corresponding uncertainties of the total cross sections are from 2% to 10%. Total transmissions are typically measured at $n\sigma x = 0.2 \div 0.4$ and result in the underestimating of the averaged group cross sections by 20% – 40% in the region of unresolved resonances. To avoid such errors, one has to take into account corrections due to resonance self-shielding effects in the averaged cross sections. The thickness of the filter-sample reduces the effects of resonance self-shielding.

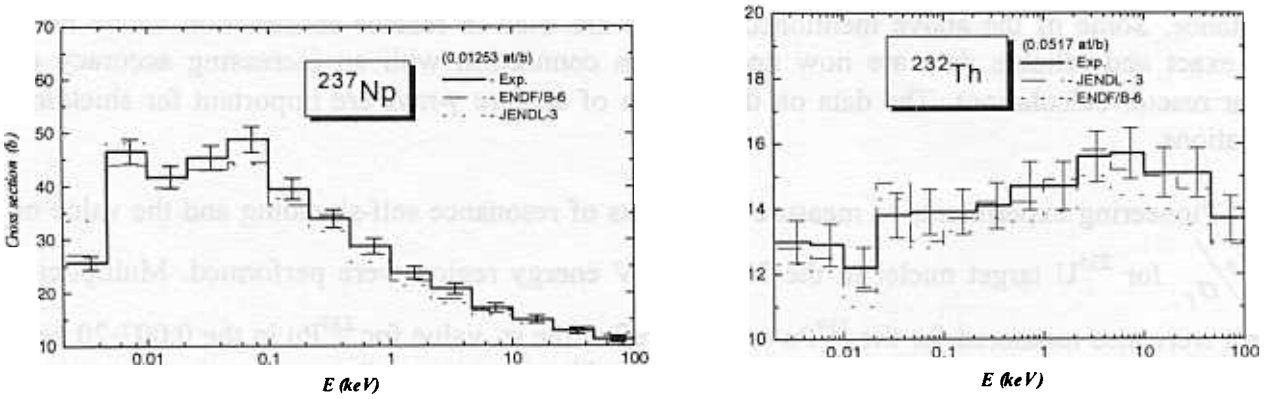


*Fig.9. The observed experimental and calculated total cross-sections of $^{237}Np$ and $^{232}Th$*

The total cross sections calculated for thick samples are in good agreement with the experimental ones as it could be seen from Fig. 9. For thin filter-samples the observed cross sections are significantly larger than for thick samples and are systematically higher than the calculated values in the energy region 2 eV–100 keV. These facts indicate conclusively that resonance structure of neutron cross sections for $^{232}Th$ and $^{237}Np$ and the corresponding resonance self-shielding have not been adequately investigated. This leads to the underestimation of the calculated cross sections in the unresolved resonance region.

## *2.6. Neutron Induced Reactions with Emission of Charged Particles*

### 2.6.1. Measurements of cross sections and angular distributions for fast neutron induced reactions

Investigations of the (n,α) and (n, p) reactions on slow neutrons continued. Processing of the data on the $^{14}N(n, p)^{14C}$ reaction completed and the results are published. The cross section measurements of the $^{35}Cl(n, p)^{35}S$, $^{36}Cl(n, p)^{36}S$, $^{36}Cl(n,\alpha)^{33}P$ reactions induced by thermal neutrons were performed using gaseous and solid targets. The processing of the angular distributions and cross sections of the $^{58}Ni(n,\alpha)^{55}Fe$ reaction at 5.1 MeV were accomplished in collaboration with Beijing and Tsinghua Universities (Beijing). The $^{64}Zn(n,\alpha)^{61}Ni$ reaction was measured for the neutron energies 5 and 6.5 MeV.

Systemizing of the (n, α) and (n, p) reaction cross-sections in the neutron energy interval from 2 to 16 MeV for the wide range of atomic weights A=19-197 was carried out. The dependence of cross sections on the (N-Z)/A parameter was obtained.

## *2.7. Astrophysical Aspects of Neutron Physics*

For a long time it has been known that abundance of elements heavier than iron in the solar-system has been produced by neutron-capture reactions. However, neutron capture is also of the relevance to abundance of isotopes lighter than iron especially to neutron-rich isotopes, even though the bulk of these elements has been synthesized in charged-particle-induced reactions. Examples of such neutron-rich isotopes that are bypassed by charged-particle reactions and are produced by neutron-induced nucleosynthesis are $^{32}Si$, $^{36}S$, $^{40}Ar$, and the calcium isotopes $^{46}Ca$ and $^{48}Ca$. Attempts to understand neutron-induced nucleosynthesis are necessary to be made to obtain important ingredients of the knowledge of neutron-capture rates. The influence of shell effects on neutron capture is one of the most interesting aspects of neutron capture, especially because neutron capture in the vicinity of magic numbers is often a bottleneck in neutron-induced nucleosynthesis. This is also the case in the neutron capture on neutron-rich isotopes close to the magic proton and

neutron numbers Z=20 and N=28, i.e., in the vicinity of the double-magic nucleus $^{48}$Ca. In particular, the reaction rate of neutron capture for Ti isotopes is of relevance to isotopic abundance anomalies in silicon carbide (SiC) grains occurring in carbonaceous meteorites. Contrary to most other solar system solids this type of grain has not been reprocessed and/or homogenized. Therefore, they can be potentially associated with their stellar origin. The main part of presolar SiC grains has an isotopic composition implying that they are most likely condensed in the winds of a variety of asymptotic giant branch (AGB) stars.

2.7.1. Neutron capture of $^{46}$Ca at thermonuclear energies

The nucleus $^{46}$Ca is produced and destroyed as a result of neutron-induced nucleosynthesis in hydrostatic helium, carbon, and neon burning through the reaction chain $^{45}$Ca(n, $\gamma$)$^{46}$Ca(n, $\gamma$)$^{47}$Ca. At the Karlsruhe and Tübingen 3.75 MeV Van de Graaff accelerators the thermo-nuclear $^{46}$Ca(n, $\gamma$)$^{47}$Ca cross section was measured by the activation technique via the 1297.09 keV $\gamma$-ray line of $^{47}$Ca decay. Samples of $CaCO_3$ enriched in $^{46}$Ca to 5% were irradiated between two gold foils serving as capture standards using the $^{7}$Li(p, n) and T (p, n) reactions. The capture cross section was measured at the mean neutron energies 30, 104, 149, 180, and 215 keV. The Maxwellian averaged capture cross sections were measured at the quasithermal neutron energies kT=25 and 52 keV. It was found that the $^{46}$Ca(n, $\gamma$)$^{47}$Ca cross section in the thermonuclear energy region and at thermal energy there dominates the s-wave resonance at 28.4 keV with the neutron width $\Gamma_n = (17.4^{+3.8}_{-2.6})$ keV and the radiation width $\Gamma_g = (2.4 \pm 0.3)$ eV. The stellar reaction rate is determined in the temperature range from kT=1 to 250 keV and is compared with previous investigations using Hauser-Feshbach calculations or experimental cross section data.

2.7.2. Neutron capture in $^{48}$Ca at thermal and thermonuclear energies

The neutron capture cross section of $^{48}$Ca was measured relative to the known gold cross section at $kT$=52 keV using the fast cyclic activation technique. The experiment was performed at the Van de Graaff accelerator of Tubingen University. The new results are in good agreement with the calculation based on a direct capture model. The $1/v$ behavior of the capture cross section at thermonuclear energies is confirmed and the adopted reaction rate which is based on several previous experimental investigations remains unchanged.

2.7.3. Measurement of neutron capture on $^{50}$Ti at thermonuclear energies

At the Karlsruhe and Tübingen 3.75 MeV Van de Graaff accelerators the thermonuclear $^{50}$Ti($n$, $\gamma$)$^{51}$Ti cross section was measured by the fast cyclic activation technique via the 320.852 and 928.65 keV $\gamma$-ray lines of $^{51}$Ti decay. Metallic Ti samples of natural isotopic composition and samples of $TiO_2$ enriched in $^{50}$Ti to 67.53% were irradiated between two gold foils that served as capture standards. The capture cross section was measured at the neutron energies 25, 30, 52, and 145 keV. The direct capture cross section was determined to be $(0.387 \pm 0.011)$ mbn at 30 keV. We found evidence of a bound state $s$-wave resonance with an estimated radiative width of 0.34 eV that destructively interferes with a direct capture. The strength of the suggested $s$-wave resonance at 146.8 keV was determined. In addition to directly measured Maxwellian averaged capture cross sections at 25 and 52 keV, the present data served to calculate an improved stellar $^{50}$Ti($n$, $\gamma$)$^{51}$Ti rate in the thermonuclear energy region from 1 to 250 keV. At low temperatures the new stellar rate leads to much higher values than the previously recommended rate; e.g., at $kT$ 58 keV the increase amounts to about 50%. The new reaction rate, therefore, reduces the abundance of $^{50}$Ti due to $s$ processing in asymptotic giant branch stars.

### *2.8. Investigations with Ultracold Neutrons*

2.8 Precise experimental test of the UCN dispersion law

In the frame of an FLNP-Kurchatov Institute-ILL-Melbourne University collaboration, a precise experiment to verify the neutron wave dispersion law was performed using an original method. It is based on a search for the resonance line shift in an interference filter, the Fabri-Perrot interferometer, accompanied with a change in the neutron velocity component parallel to the filter surface. The parameters of the spectrometer permit one to measure the shift of the resonance line ($6.5 \cdot 10^{-9}$ eV width) with the accuracy $10^{-11}$ eV.

Deviations from the dispersion law were not observed on such a level.

2.8.2. Observation of the new mechanism of UCN losses

UCN can be confined in material traps for a long time making possible their usage in experiments aimed at studying the fundamental properties of the neutron. It is well known that, in particular UCN losses in traps are due to β-decay, upscattering and capture on the trap walls. In the reported study an additional mechanism of UCN escape from traps was observed. It is associated with an approximately two-fold increase of UCN energy with a probability of about $10^{-6}$ per collision for the stainless steel surface and it is lower for other studied materials (Cu, Be). The observed effect does not reduce to known UCN upscattering that leads to an increase in the neutron energy to approximately thermal energy.

## 3. Theoretical Researches

### *3.1. Nuclear Fission*

A theory of nuclear fission induced by resonance neutrons was developed. The new and sufficiently natural interpretation of A. Bohr's fission channels follows from this theory. A unified description of P-even and P-odd angular correlations of fission fragments has been made. Part of the predicted new effects found confirmation in the experimental works performed in FLNP (see sections 2.4.1, 2.4.2). This theoretical approach was used for an analysis of the experimental data on the resonance neutron induced fission of aligned $^{235}$U target nuclei.

### *3.2. Neutron optics*

The reflection of neutrons from multilayer magnetic systems was considered numerically and analytically. The magnetization of adjacent layers was supposed to be noncollinear. Two methods were compared. The first one, analytical, uses infinitesimal splitting of layers and multiple reflections in the infinitesimal gaps. It is analytical and is called the recursion method (RM).

The second one uses matching of the wave function at the interfaces of layers. The wave function is represented as a two-dimensional vector, $\psi = \begin{pmatrix} \psi_0 \\ \rho\psi_0 \end{pmatrix}$, or $\psi = \begin{pmatrix} \tau\psi_0 \\ 0 \end{pmatrix}$ with both components being spinors. Here $\psi_0$ is the incident spinor wave, and $\rho$, $\tau$ are the reflection and transmission amplitudes, respectively. The upper component is related to the wave going right and the lower one is the wave going left. Matching at the i-th interface is described with a generalized 2x2 matrix (GM) $M_i$: $\psi_i = M_i\psi_{i-1}$, with the matrix elements of $M_i$ being 2x2 matrices. The GM provides the continuity of the wave function and its derivative. Successive matching at different interfaces gives the resulting matrix from which the reflection spinorian amplitude can be evaluated. This method, called the generalized matrix method (GMM), is appropriate for numerical calculations.

A comparison of two methods in numerical calculations has shown that GMM is less time consuming. It is nearly 10 times faster than RM. However, RM has an advantage if we only need to find the positions and width of resonances in a multilayer system.

### *3.3. Neutron-electron interaction*

The neutron-electron scattering amplitude $a_{ne}$ is usually extracted from transmission experiments where the transmission exponent *exp (-Nσ$_t$L)* of the sample is measured. Here, *N* is the atomic density, *L* is the thickness of the sample, and $\sigma_t$ is the total transmission cross section which contains the coherent elastic scattering cross section $\sigma_{el}^c$. It is the latter which is most important for $a_{ne}$, because $\sigma_{el}^c = \int d\Omega |a_c - Z a_{ne} f(q)|^2$, where $a_c$ is the coherent neutron-nucleus scattering amplitude, *Z* is the atomic number, *f (q)* is the atomic form factor which depends on the momentum transfer *q*, and the integration should be performed over all scattering angles *Ω*. Since the amplitude $a_{ne}$ is small, the last expression can be approximated as $\sigma_{el}^c = \sigma_0^c \left[1 - 2Z\left(a_{ne}/a_c\right)\langle f(k)\rangle\right]$, where $\sigma_0^c = 4\pi|b_c|^2$, *k* is the wave number of the incident neutrons, and $f(k) = \int d\Omega \, f(q)/4\pi$ is the form-factor averaged over all angles. Thus, to find $a_{ne}$, we need to measure $\sigma_{el}^c$, the dependence $\sigma_{el}^c(k)$ on *k* and also, know <*f (k)*>.

However, it is shown that at small *k* the coherent cross section $\sigma_{el}^c$ does not enter into $\sigma_t$ at all, and in the case of polycrystalline media, at large *k* this cross section enters into the Placek correction, i.e. $\sigma_t$ contains $\sigma_{el}^c\left(1 - C/a^2k\right)$, where *C* is the constant calculated by Placek and *a* is the interatomic distance. It is seen that the Placek correction $C/a^2k^2$ increases as *k* decreases, but it is not clear how it completely eliminates $\sigma_{el}^c$ at small *k*.

It was shown that:

1. the contribution of $\sigma_{el}^c$ taking into account the Placek correction can be represented in the form $\sigma_{el}^c\left[1 - 1/\left(1 + a^2k^2/C\right)\right]$, which is acceptable for all *k*.
2. the magnitude of the Placek constant has some uncertainty which depends on the form of the atomic correlation function and leads to an uncertainty in the $a_{ne}$ magnitude of the order of 10\%.
3. the correction to $\sigma_{el}^c$ at large *k* also contains the term $\approx \left(4/ka\right)\left(l/a\right)\left(b_c/a\right)$, where *l* is an average dimension of crystallites.

Some corrections which can modify the amplitude related to the neutron polarizability were also considered.

### *3.4. Ultracold neutrons*

Attempts were made to explain the anomaly of ultracold neutrons fom the fundamental viewpoint. An assumption was made that a non-spreading wave packet can describe the neutron and a reduction of the wave function takes place both in the coordinate and momentum space. It has also been noticed that a particle and its wave function are a non-local object whose coordinates and momentum demand an exact mathematical determination and can be determined unambiguously

and simultaneously without coming in contradiction with the uncertainty principle which appears to have no relation to quantum mechanics. In the frame of the canonical approach, one fails to describe anomalous losses. In the frame of de Broglie representations, a singular wave packet can be ascribed to the neutron. In this case, the anomaly can be explained by over-barrier leakage. As a result, the packet width is determined, the future of the neutron is predicted, and the possibility of experimental verification of this prediction is hoped for.

Experiments to verify the hypothesis started in 1998 and continued in 1999 in collaboration with Kyoto University (Japan) and Institute Laue-Langevin (France).

## 4. Methodological Researches

### *4.1. The anticompton gamma spectrometer HPGe-BGO for nuclear physics experiments at pulsed neutron sources*

Pioneer investigations to observe the neutron standing waves using the TOF technique with a high precision gamma-spectroscopy were performed on channel 8 of the IBR-2 reactor.

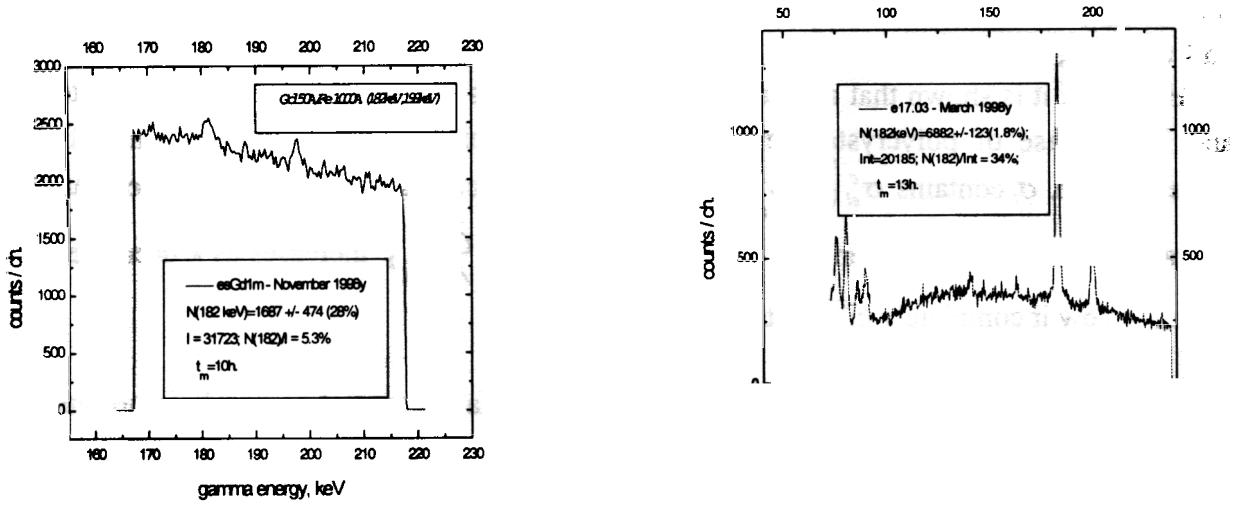


*Fig.10. Gamma- spectra from $^{158}Gd$ in a multilayer structure without anticompton spectroscopy (left) and with anticompton spectroscopy (right)*

The technique determines the success in the studying of the long wave dependence of the neutron density in layers with an extremely high capture cross section (Gd, Sm, Cd) and a several angstrom thickness. This permits one to discover such elements in a multilayer structure and determine their spatial position.

Figure 10 demonstrates improvements in the use of the technique after applying a high precision gamma- spectroscopy with an anticompton active shielding.

### *4.2. Construction of the KOLHIDA instrument*

To carry out investigations of the paramagnetic neutron resonance and nuclear pseudomagnetism on the IBR-2 pulsed reactor, an experimental complex "Kolkhida" is being built which consists of a polarized neutron spectrometer and a polarized nuclear target installation. The spectrometer for investigations with polarized neutrons has been completed and measurements of its parameters have been carried out.

The spectrometer of polarized neutrons is located on the first channel of IBR-2. The general scheme of the spectrometer is shown in Fig. 11. The Co(92%)-Fe(8%) single crystals (1 and 2) are used for neutron polarization and polarization analysis.

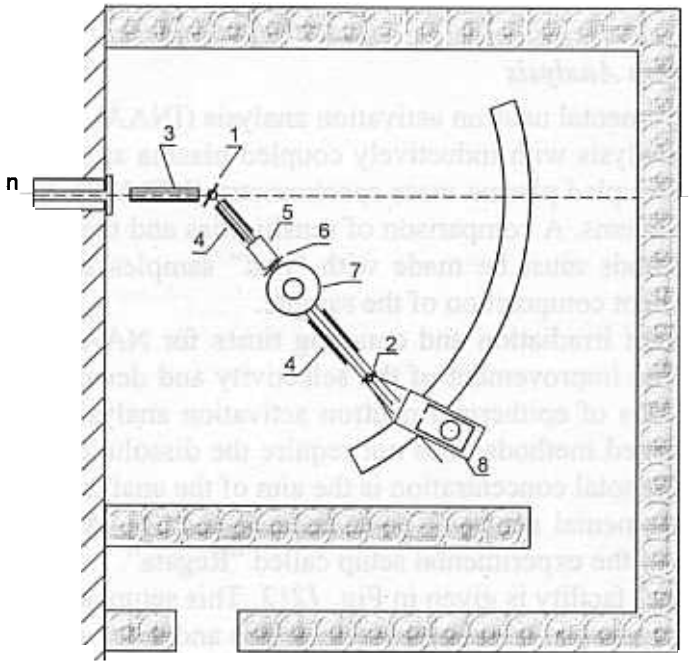


*Fig.11. A schematical view of the Kolkhida setup. 1,2 – Co-Fe crystals; 3 - collimator; 4 – magnet; 5 – spin flipper; 6 – fission chamber monitor; 7 – polarized target; – neutron detector*

The thickness of the crystals is 3 mm and the surface areas are 34x34 $mm^2$ and 35x53 $mm^2$, respectively. The crystals are placed between the poles of the electromagnets which produce a magnetic field of H=0.4T.

The spectrometer is assembled on a massive arm. It comprises guide field magnets (4), a flipper (5) for polarization reversal, a polarized target holder (7), a polarization analyzer (2) with a magnet, and a platform with a neutron detector (8). The arm on a circular rail can be rotated about the same axis as the neutron polarizer. The rotation axis of the detector platform coincides with the axis of the neutron analyzer. The $^3$He counter is used as a neutron detector and the $^{235}$U fission chamber (6) is used to monitor the primary neutron beam.

The parameters of the polarized neutron beam are given in Table 3.

*Table 3*

**The parameters of the polarized neutron beam**

| Angle $\theta$ (degree) | 19 | 12 | 6 | 4 | 3 |
|---|---|---|---|---|---|
| Wavelength $\lambda$ (Å) | 1,15 | 0,74 | 0,37 | 0,25 | 0,19 |
| Energy $E_n$ (eV) | 0,062 | 0,15 | 0,60 | 1,3 | 2,3 |
| Counting rate of the detector behind the polarizer, $n_1$ ($sec^{-1}$) | 800 | 270 | 65 | 33 | 22 |
| Intensity of polarized neutrons $I_1$ (n/sec $cm^2$) | 430 | 200 | 80 | 60 | 50 |
| Counting rate of the detector after analysis $n_2$ ($sec^{-1}$) | 70 | 23 | 3,1 | 0,6 | 0,2 |

The completed tests of the spectrometer showed that it could be used conveniently to carry out investigations with polarized neutrons over a range from thermal energy to several eV.

# 5. APPLIED RESEARCH

## *5.1. Neutron Activation Analysis*

At the present time, instrumental neutron activation analysis (INAA) is one of the most sensitive methods for multielement analysis with inductively coupled plasma atomic emission spectrometry (ICP-AES) and inductively coupled plasma mass spectrometry (ICP-MS). Each of these techniques has their own merits and problems. A comparison of sensitivities and the quantity of elements to be determined for various methods must be made with "real" samples because the analysis result depends strongly on the element composition of the sample.

A combination of different irradiation and counting times for NAA technique is necessary to achieve an optimal result. The improvement of the selectivity and detection power of this method can be also achieved by means of epithermal neutron activation analysis (ENAA). Besides NAA, just one of the above mentioned methods does not require the dissolution of the sample. This is a great advantage of NAA if the total concentration is the aim of the analysis.

Applications of the instrumental neutron activation analysis (INAA) at the IBR-2 fast pulsed reactor are based on the use of the experimental setup called "Regata".

The layout of the "Regata" facility is given in Fig. *1*212. This setup consists of four channels for irradiation (Ch1-Ch4), the pneumatic transport system (PTS) and three gamma-spectrometers. It is located in three special rooms on the ground floor of the reactor IBR-2 building. The main parameters of the irradiation channels are presented in Table 4. The channels Ch3, Ch4 are cooled with water and the channels Ch1 and Ch2 connected with the pneumatic transport system are cooled with air. That is why the temperature in channels Ch3 and Ch4 is less than the temperature in channels Ch1 and Ch2 with the greater fluxes of neutrons. The time of sample irradiation in channels Ch3, Ch4 depends on the operation cycle duration of the reactor and is equal to 10-12 days, as a rule.

*Table 4*

**Irradiation channel parameters**

| Irradiation site | Neutron flux density ($n/cm^2 s$)$\times 10^{12}$ | | | T°C | Channel diam., mm | Channel length, mm |
|---|---|---|---|---|---|---|
| | Thermal | Resonance | Fast | | | |
| Ch1 | Cd coat | 0.23±0.03 | 1.4±0.16 | 70 | 28 | 260 |
| Ch2 | 0.54±0.06 | 0.12±0.01 | 0.64±0.04 | 60 | 28 | 260 |
| Ch3 | Cd coat | 4 | 7.0±0.5 | 30-40 | 30 | 400 |
| Ch4 | 13.0±0.5 | 0.9±0.10 | 7.0±0.5 | 30-40 | 30 | 400 |
| Ch0 | $n_o \cong 0$ | 1.25±0.1 | 150 | 400 | 16 | 180 |
| | | <0.1 | | | | |

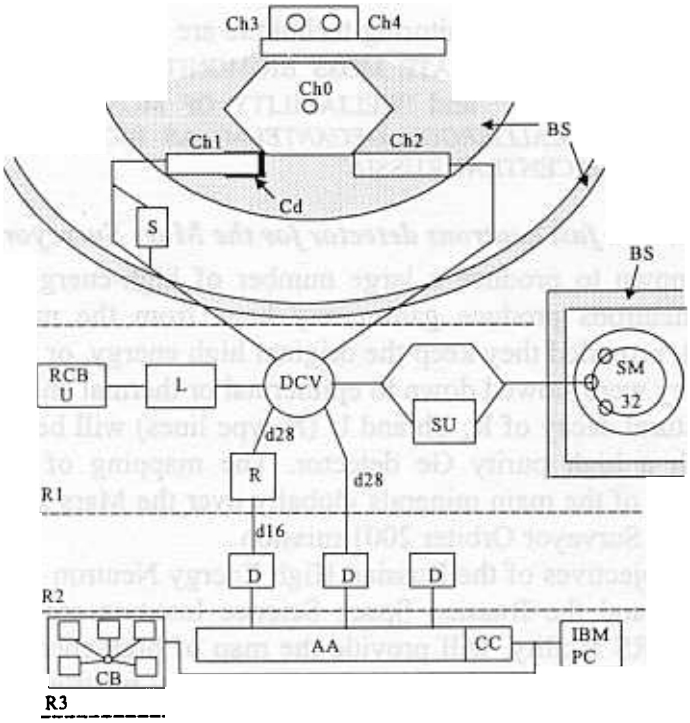


*Fig. 12. The scheme of the "Regata" experimental setup. Ch0-Ch4 –irradiation channels, S- intermediate storage, DCV- directional control valves, L- loading unit, RCB- radiochemical box, U- unloading unit, SU- separate unit, SM- storage magazine, R- repacking unit, D- Ge(Li) detector, AA- amplitude analyzer, CB- control board, CC- controller CAMAC, R1-R3- The rooms where the system is located.*

The irradiation channels Ch1 and Ch2 are the same, but Ch1 has a Cd coating. Each channel consists of two concentric tubes made from stainless steel. Both are placed into an aluminum box with a biological shield. One of the tubes is a flight tube 28 mm in diameter, and compressed air flows through the second tube. In order to prevent a hard shock of a capsule with the irradiated sample at the end of the channel there is an additional valve to let the compressed air out.

In the reported period most experience in applying the activation analysis involves air pollution studies in some industrial areas of Russia (the South Ural, Tula, Moscow region) and in member-states of JINR (Poland, Romania). The application of the neutron activation analysis with epithermal neutrons (ENAA) allows improving of the selectivity and detection power of the method. The technique is based on the fact that some elements have isotopes with resonances in the epithermal neutron region. The ratio of resonance activation integral/thermal neutron cross-section ($I_o/\sigma_o$) is of the order of 0.5 for nuclides without resonance in the epithermal neutron region and it may be as high as 100 in other cases. This means that the radionuclide distribution originating from epithermal activation may deviate strongly from the apparent when the whole reactor spectrum is employed. This forms the basis of ENAA.

The dominant part of air pollution studies is based on the use of the moss biomonitoring technique. Mosses have no developed root system that is why they take nutrients almost exclusively from the atmosphere. This technique has been applied to study air pollution with heavy metals and other trace elements in combination with the atomic absorption spectrometry of the elements Pb, Cd, Cu and Ni. The results of the investigations are presented in the form of tables, diagrams, graphs and, using the geographical information system (GIS) technology, in the form of colored contour maps for each element. The technique of multivariant statistical analysis (factor analysis) is applied to obtain information on the character and origin of pollution sources.

In more detail, the NAA and biomonitoring technique are presented in the section of scientific publications: "SELECTION OF APPROPRIATE MOSS BIOMONITORS FOR STUDYING ATMOSPHERIC ELEMENTAL DEPOSITION IN CHINA" and "RELIABILITY OF MOSSES *(HYLOCOMIUM SPLENDENS, PLEUROZIUM SCHREBERI* AND *CALLIERGON GEGANTEUM)* AS BIOMONITORS OF HEAVY METAL ATMOSPHERIC DEPOSITIONS IN CENTRAL RUSSIA"

### *5.2. Development of a fast neutrons detector for the Mars Surveyor 2001 space program*

Cosmic rays are known to produce a large number of high-energy neutrons in the Martian surface layer. These neutrons produce gamma-ray lines from the nucleus either via inelastic scattering (I-type lines), provided they keep the original high energy, or via capturing reactions (C-type lines), provided they were slowed down to epithermal or thermal energies. These lines together with the lines of the natural decay of K, Th and U (N-type lines) will be measured by the Gamma-Ray Spectrometer with a high purity Ge detector. The mapping of these lines will allow to determine the distribution of the main minerals globally over the Mars surface, which is one of the primary goals of the Mars Surveyor Orbiter 2001 mission.

The main scientific objectives of the Russian High Energy Neutron Detector HEND created by a collaboration of JINR and the Russian Space Science Institute are consistent with this goal. HEND, as part of the GRS facility, will provide the map of high-energy neutrons albedo, which will allow (together with a complementary map of low energy neutrons albedo from the Neutron Spectrometer NS) the distinguishing of I-type, C-type and N-type lines from a "forest of lines" from the GRS spectrometer.

To achieve these goals, HEND is integrated into GRS. The HEND detector scheme was developed, modeled, and tested in FLNP. It has three $^{3}$He-based neutron counters with polyethylene moderators and one stylben scintillator with an active anti-coincidence shielding around it. The $^{3}$He-based detectors with thin and medium moderators will ensure the complementary measurement verification in the Neutron Spectrometer at low energies below 1 keV, and will provide data for the cross-calibration of HEND and NS. The $^{3}$He-based detector with a thick moderator and a stylben scintillator will provide data for high energy neutrons at 1 keV–10 MeV to build a map of the elemental composition of the Martian surface and determine regions with an increased abundance of hydrogen on a shallow subsurface.

Also, the data of high-energy neutrons from HEND will characterize the radiation environment on the interplanetary cruise and on the Martian orbit to provide information about radiation-related risks to human explorers. Special data formats with time profiles will be used to measure, with a fine time resolution, the fluxes of high-energy neutrons and gamma rays during strong solar flares and gamma ray bursts.

The numerical computation of the detectors sensitivity was performed in FLNP to optimize the thickness of the moderators around the $^{3}$He-counters for the expected energy spectra of albedo neutrons on the Martian orbit. The instrument will be calibrated in the neutron beams of the Van de Graaf accelerator and the pulsed neutron reactors of FLNP. The cross-calibration of the HEND and NS in the overlapping range of neutron energies will be performed by means of numerical computations.